PHYSICAL REVIEW B **83**, 121305(R) (2011)

Ripple rotation in epitaxial growth of MnAs(1$\bar{1}$00)

F. Vidal,[1] V. H. Etgens,[1] V. Fernandes,[1,2] B. Rache Salles,[1,*] and M. Eddrief[1]

[1]*Institut des NanoSciences de Paris, UPMC, CNRS UMR 7588, 4 place Jussieu, F-75252 Paris Cedex 05, France*

[2]*Instituto Federal de Educação, Ciência e Tecnologia do Paraná–Campus Curitiba, 80230-150 Curitiba, PR, Brazil*

(Received 13 January 2011; revised manuscript received 25 February 2011; published 15 March 2011)

Rippled states formation driven by kinetic instability is evidenced in the case of MnAs(1$\bar{1}$00) hetero- and homoepitaxial growth in a narrow multistable range of growth parameters. The evolution of the surface morphology in this range, comprising slope selection and ripple rotation, maps the kinetic phase diagram recently predicted [A. Levandovsky and L. Golubović, Phys. Rev. E **76**, 041605 (2007)] for growth on rectangular symmetry surfaces, including Ehrlich-Schwoebel instability and effects related to vertical asymmetry.

DOI: 10.1103/PhysRevB.83.121305 PACS number(s): 68.55.−a, 68.35.Fx, 68.37.Ef, 81.15.Hi

Thin-film epitaxial growth is at the core of an increasing number of applications in electronics, photonics, spintronics, etc. It is a fundamentally out-of-equilibrium process and, as such, is subjected to kinetic instabilities. Recently these instabilities have been studied extensively in the simplest case of homoepitaxial growth of cubic metals, and can lead to fascinating patterned morphologies of the growth front with mound shapes following the symmetry of the crystalline surface.[1] In the case of homoepitaxial growth on the rectangular (110) surface of cubic compounds, rippled states—wavelike one-dimensional periodic structures—have been observed for several simple fcc and bcc metals such as Ag,[2] Cu,[3] Ni,[4] and Fe.[5] This self-organization can be exploited for applications requiring substrates with specific morphology in plasmonics[6] or nanomagnetism.[7,8] Thus, the seemingly simple problem of homoepitaxial and erosion of cubic metals is still intensively studied, both experimentally and theoretically.

The ripple formation originates from the Ehrlich-Schwoebel (ES) barrier, an extra energy barrier felt by adatoms at steps where they bounce back instead of reaching lower terraces.[9,10] Because of the ES barrier, diffusion is perturbed in directions perpendicular to the steps, and this eventually leads to growth instabilities due to suppressed interlayer mass transport and a resulting net uphill current perpendicular to the steps direction. Following pioneering works,[11] continuum models have been refined recently and the models now allow to reproduce the main experimental trends observed, including ripple rotation, a sharp change of 90° in the orientation of the pattern when varying the growth temperature, in the case of fcc (110) surfaces.[12] Within such models, h, the height of the growth front obeys the following equation:

$$\partial h(\vec{x},t)/\partial t = v(h) = -\vec{\nabla}\cdot\vec{j}, \tag{1}$$

where j is the surface current that can be split into three terms having distinct origins:

$$\vec{j} = \vec{j}_{\rm sd} + \vec{j}_{\rm ne}(\vec{\nabla}h) + \vec{j}_{\rm va}. \tag{2}$$

$\vec{j}_{\rm sd}$ is the classical diffusion current. $\vec{j}_{\rm ne}$ is the nonequilibrium current that leads to Ehrlich-Schwoebel-Villain instabilities with mound and/or ripple formation and possible slope selection (corresponding to values of $\vec{\nabla}h$ for which $\vec{j}_{\rm ne}$ vanishes) and, therefore, growth of facets on the initially nominal surface. $\vec{j}_{\rm va}$ is the current related to vertical asymmetry, i.e., the fact that in general there is no reason to have the vertical reflection ($h \to -h$) symmetry for the growing surface: $v(-h) \neq -v(h)$. It has been shown recently that this last term has to be taken into account in order to describe in detail the ripple rotation phenomenon.[12]

So far, ripple formation has been addressed only in the case of simple cubic metals. In this paper, we study the case of MnAs, a ferromagnetic hexagonal compound [Fig. 1(a)] and evidence ripple formation and rotation during (1$\bar{1}$00)-oriented epitaxial growth. The obtained morphologies are in close agreement with recent simulations, including Ehrlich-Schwoebel-Villain instabilities and vertical asymmetry effects. This extends the range of compounds subject to such kinetic pattern formation that could—in the present case—be explored in the field of nanomagnetism.

MnAs has been much studied in recent years because of its compatibility with III-V compounds,[13] which could be exploited in the framework of spintronics,[14] and interesting magnetostructural properties.[15–17] Due to the peculiar phase transition sequence of MnAs, striped elastic domain formation can lead to a modulation of the MnAs/GaAs (001) surface around room temperature.[18] Here, we focus exclusively on the growth morphology that is independent of such elastic modulation.[19]

MnAs single-crystal epilayers were grown on GaAs(001) substrates by molecular-beam epitaxy in a Riber Compact 21 system. Substrates were deoxidized under As flux, and a GaAs buffer layer was grown subsequently at 850 K under As-rich conditions in order to achieve optimal surface quality. MnAs epilayers were then grown on GaAs $c(4\times4)$ reconstructed surfaces (heteroepitaxy) or on prepared MnAs (1$\bar{1}$00) flat surfaces (homoepitaxy). The growth temperature (T_g) was in the 480–590 K range. The MnAs/GaAs(001) epitaxial relation, illustrated in Fig. 1(b), was checked by reflection high-energy electron diffraction and x-ray diffraction. MnAs samples display a single domain epitaxy with the hexagonal [0001] axis parallel to the [1$\bar{1}$0] direction of the GaAs (001) template. Scanning tunneling microscopy (STM) data were acquired in a VT-STM apparatus (Omicron nanotechnology) connected under UHV to the growth chamber. The image were recorded in constant current mode with 1 V bias and current in the 20–100 pA range at room temperature. STM data were analyzed using WSxM software.[20]

In the temperature range investigated here, the atomic scale of MnAs (1$\bar{1}$00) is well documented.[21,22] Under such

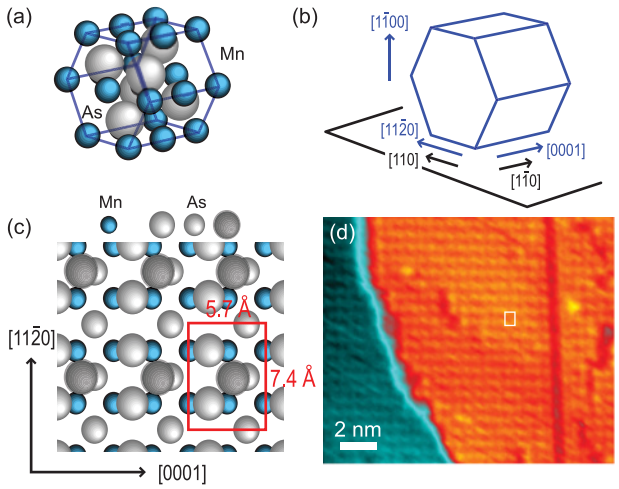

FIG. 1. (Color online) (a) NiAs-type crystal structure of α-MnAs consisting of hexagonal planes of Mn and As. (b) Epitaxial scheme of MnAs on GaAs(001). (c) Ball model of the (1×2) MnAs(1$\bar{1}$00) surface reconstruction, adapted from Ref. 22. (d) STM image of the (1×2) reconstruction. The line defect at the right-hand side of the image is assigned to an antiphase boundary between two reconstructed domains.

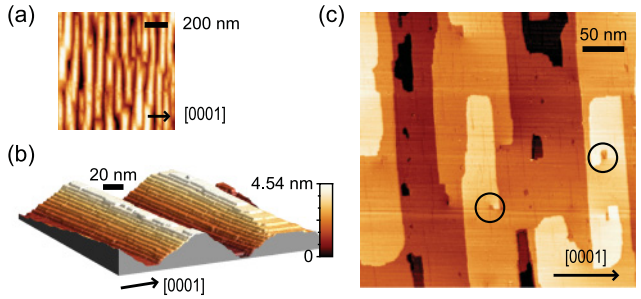

FIG. 2. (Color online) (a) STM image of 150-nm-thick MnAs grown at $T = 540$ K, evidencing ripple formation. (b) Zoom in on the ripple morphology shown in (a). Terrace piling and slope selection lead to the formation of elongated pyramids. (c) STM image of MnAs grown at higher temperature, $T = 588$ K. Circles indicate some of the screw dislocations observed.

conditions, the surface adopts a (1 × 2) reconstruction with a rectangular symmetry [see the ball model in Fig. 1(c)]. Figure 1(d) shows a typical high-resolution image evidencing such (1 × 2) reconstruction. Given the rectangular symmetry of the surface and, consequently, potentially distinct diffusion and ES barriers along [0001] and [11$\bar{2}$0], the question that arises is: Are the ingredients necessary for rippled state formation during growth gathered? The answer is yes: Quasiperiodic ripples, with lengths up to several hundreds of nanometers, can be clearly observed in STM images of a 150-nm-thick MnAs epilayer grown at 540 K, reproduced in Fig. 2(a). Higher-resolution imaging [Fig. 2(b)] reveals the local structure of these ripples: They are made by a piling of highly anisotropic elongated terraces (with step heights of 3.2 ± 0.2 Å) running perpendicular to [0001]. Such morphology results from limited diffusion along [0001] and indicates that kinetic limitations may occur during the growth, most notably that thermal energy may not be sufficient to cross the ES barrier in the [0001] direction. Indeed, results obtained for growth at higher temperatures, as well as after annealing steps, confirm this view. Figure 2(c) shows the morphology after growth at 588 K: The surface is quite flat with large terraces, and dislocations with a screw component along the surface normal appear. This indicates that thermal energy is sufficient to overcome the diffusion and ES barriers. The growth regime then evolves from kinetically limited growth (due to impeded interlayer mass transport along [0001]) to spiral growth at higher temperatures.

In order to determine the effect of T_g, we studied the growth front morphology systematically after homoepitaxial growth steps (deposited thickness 30 nm) performed at various temperatures on a flat MnAs (1$\bar{1}$00) surface. The results of such an investigation are summarized in Fig. 3. At low temperatures, the surface is paved with mounds elongated

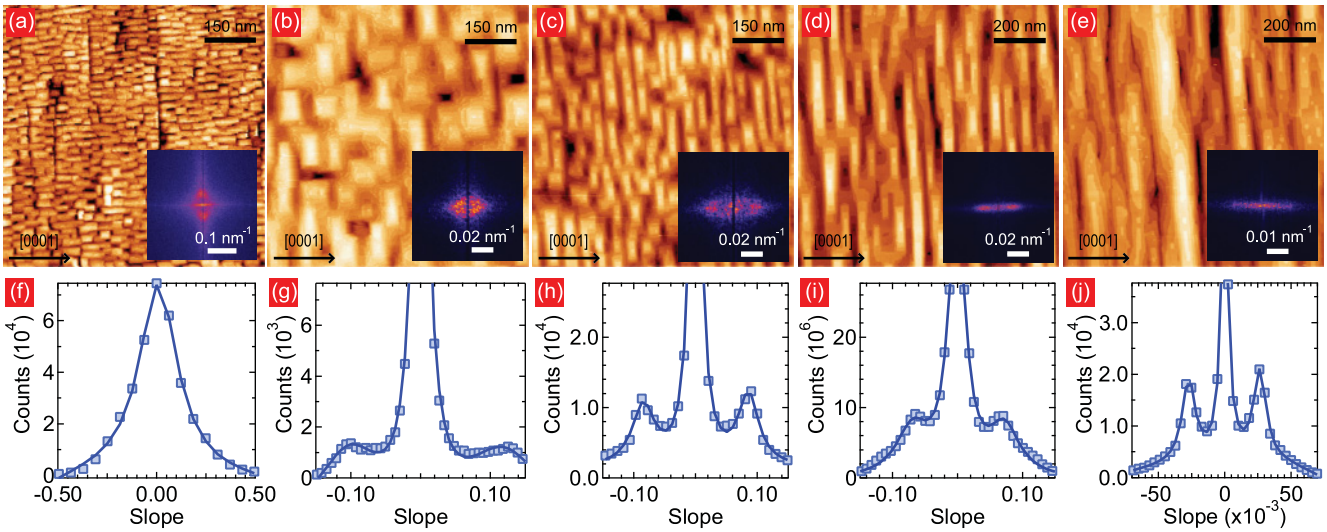

FIG. 3. (Color online) (a)–(e) STM images and corresponding FT patterns of MnAs (1$\bar{1}$00) growth front for $T_g = 488$ K (a), 521 K (b), 538 K (c), 555 K (d), and 563 K (e). (f)–(j) Slope distribution along [11$\bar{2}$0] for $T_g = 488$ K (f), along [0001] for $T_g = 521$ K (g), 538 K (h), 555 K (i), and 563 K (j).

in the [0001] direction [Fig. 3(a)]. Although their size is limited and their shape is not regular, due to limited diffusion, there is a clear anisotropy. The Fourier transform (FT) of STM images, displayed in the inset of Fig. 3(a), exhibits a clear twofold symmetry with two lobes pointing along [11$\bar{2}$0]. Increasing T_g to 521 K leads to a drastic change of the growth front morphology: As shown in Fig. 3(b), rectangular mounds arranged in a checkerboard pattern can be observed. The FT now has a fourfold symmetry with lobes pointing in both [11$\bar{2}$0] and [0001] directions. A further increase of T_g beyond 521 K leads to a recovering of the twofold symmetry, but the FT pattern is rotated by 90° with respect to the orientation prevailing at lower temperature [insets in Figs. 3(c)–3(e)]. For $T_g = 538$ K, elongated mounds aligned in the [11$\bar{2}$0] direction decorate the surface [Fig. 3(c)]. A subsequent increase of T_g leads to the appearance of a well-developed ripple pattern with ridges running along [11$\bar{2}$0] [Figs. 3(d) and 3(e)]. We thus observe ripple formation and rotation (with a checkerboard intermediate state) in the 488–563 K growth temperature range. Performing growth beyond this range leads to flat surfaces with large terraces—see Fig. 2(c).

Local slope distributions, obtained from STM images, are displayed in Figs. 3(f)–3(j), evidencing slope selection: The

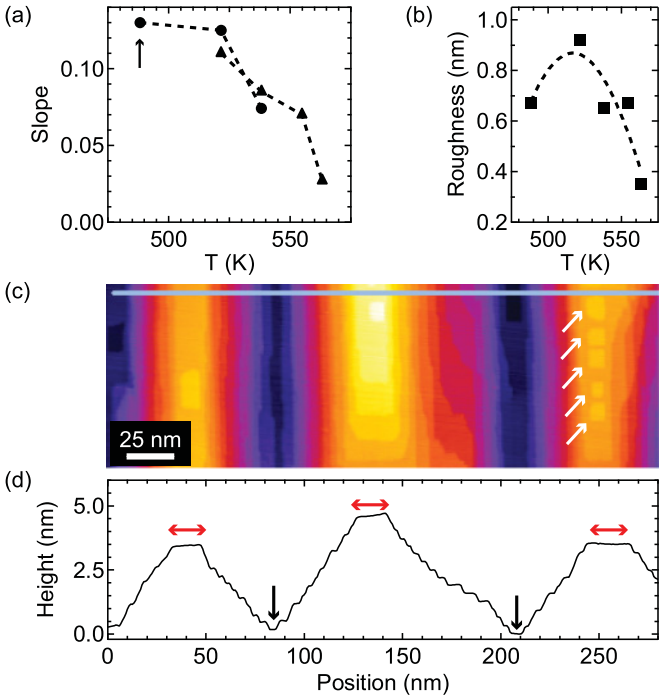

FIG. 4. (Color online) (a) Selected slope along [11$\bar{2}$0] (dots) and along [0001] (triangles) as a function of the temperature, extracted from slope distributions measured on the MnAs(1$\bar{1}$00) growth front. The point marked by an arrow at the lowest temperature is the half width of the slope distribution depicted in Fig. 3(f), for which no peak (except the central one) could be resolved. (b) Roughness (rms value) as a function of the temperature. (c) STM image of 150-nm-thick MnAs grown at $T = 540$ K. The arrows point toward islands decorating rooftops. (d) Height profile obtained along the line drawn in the STM image of (c). Vertical arrows locate pits with a depressed lateral extension as compared to rooftops, whose location is highlighted by horizontal double arrows.

projection of $\vec{\nabla} h$ along the [11$\bar{2}$0] and [0001] directions peaks at well-defined values that depend on T_g. The evolution of the selected slopes—along [11$\bar{2}$0] and [0001]—as a function of the temperature is plotted in Fig. 4(a). In the temperature range corresponding to the 90° rotation of the ripples, slope selection occurs in both directions and a crossing of the selected slopes is observed. We will come back to this particular point in what follows. Globally, the slopes decrease with increasing temperature: Enhanced diffusion at high T_g leads to a smoother growth front.

In the continuum description of kinetic instabilities, such a slope selection is linked to the ES barriers and is encoded in the related current $\vec{j}_{\rm ne}$ that vanishes for a given value of the local slope.[11,12] This is a clear fingerprint, and we thus discuss our results in terms of diffusion barriers and then in the framework of continuum models in what follows.

Although the situation is more complicated in the case of MnAs, a biatomic compound, than for a simple metal, it is possible to explain the ripple formation and rotation by considering elementary diffusion processes, as in the case of Ag(110).[2] Intralayer diffusion is governed by energy barriers $E_{d[0001]}$ and $E_{d[11\bar{2}0]}$, and interlayer transport by step-edge barriers $E_{s[0001]}$ and $E_{s[11\bar{2}0]}$. The hierarchy of these barriers and the amount of thermal energy available determines which process is frozen or not at a given temperature. It is then possible to define activation temperatures related to the energy barriers $T_{d[0001]}$, $T_{d[11\bar{2}0]}$, $T_{s[0001]}$, and $T_{s[11\bar{2}0]}$. In close analogy with the case of Ag(110), we suppose the following peculiar hierarchy for the activation temperatures: $T_{d[11\bar{2}0]} < T_{s[11\bar{2}0]} < T_{d[0001]} < T_{s[0001]}$. Then the ripple formation and rotation can be understood as follows. For $T_{d[11\bar{2}0]} < T_g < T_{s[11\bar{2}0]}$, intralayer diffusion along [11$\bar{2}$0] is possible but $E_{s[11\bar{2}0]}$ cannot be crossed, and the additional ES barrier results in an uphill current perpendicular to the steps oriented along [0001]: Ripple formation along [0001] is then favored. Increasing T_g toward $T_{d[0001]}$ has two consequences: (i) Diffusion along [0001] becomes easier but $E_{s[0001]}$ cannot be crossed, and there is an uphill current perpendicular to [0001]; (ii) since the thermal energy available increases, the uphill current perpendicular to [11$\bar{2}$0] decreases. Combined together, these currents lead to the appearance of rectangular mounds arranged in a checkerboard pattern, with slope selection in both directions. Then, for $T_{d[0001]} < T_g < T_{s[0001]}$, all processes are allowed except crossing $E_{s[0001]}$: The uphill current perpendicular to [11$\bar{2}$0] steps leads to ripple rotation by 90° with respect to the direction favored at low temperature. Further discussion of the microscopic processes involved in MnAs growth would require some insight from, e.g., a molecular dynamics simulation, and we hope that our results will motivate such investigation.

Coming back to the continuum model description, recent work by Levandovsky and Golubović shows that ES barriers, which are key ingredients to explain ripple formation and rotation, are not sufficient to describe satisfactorily the growth front morphology: This can only be done by including vertical asymmetry effects.[12] The latter give rise to some clear fingerprints such as (i) the FT lobes point along [11$\bar{2}$0] and [0001] directions and *not along diagonal directions* for the checkerboard state that forms in the slope crossing region,

(ii) the maximal surface roughness is reached in that same crossing region, and (iii) the appearance of a wormlike state, labeled Alt$R_2^{(\mathrm{rec})}$ in Ref. 12, after the crossing region, on the declining slope side. This Alt$R_2^{(\mathrm{rec})}$ state is characterized by very elongated ripples, depressed pits as compared to rooftops, and it is predicted that small islands can be found on the rooftops. These fingerprints are clearly present in our detailed STM study: (i) In Fig. 3(b), (ii) in Fig. 4(b) and (iii) in Fig. 2(a), where wormlike ripple formation is evidenced, and in Figs. 4(c) and 4(d), where depressed pits compared to wider rooftops, as well as rooftop decoration by islands are all observed. Indeed, the evolution of MnAs morphology with T_g maps the kinetic phase diagram depicted in Fig. 5 of Ref. 12 once the smoothing effects of diffusion (that increase with T_g) are taken into account. This provides strong support in favor of the predicted importance of vertical asymmetry effects in the continuum description of epitaxial growth.

In this paper, we have evidenced ripple formation and rotation for a binary compound. The evolution of MnAs morphology can be explained in the framework of kinetic instabilities related to ES barriers and vertical asymmetry, as described recently in a theoretical work.[12] This shows that the concepts applied to describe kinetic instabilities in the growth of simple model materials can be extended to other class of more complex materials. Finally, we stress that patterned MnAs anisotropic surfaces were exploited recently as a template for nanomagnetism studies: Fe/MnAs/GaAs(001) were shown to exhibit peculiar magnetic properties.[23,24]

The authors acknowledge the support of the French Agence Nationale de la Recherche (ANR), project GIFAD, of CAPES-COFECUB Program, and of CNPq.

*Present address: Spintronics Research Center, AIST, Tsukuba Central 2, Umezono 1-1-1, Tsukuba Ibaraki 305-8568, Japan.

[1] T. Michely and J. Krug, *Islands, Mounds, and Atoms: Patterns and Processes in Crystal Growth Far from Equilibrium*, Springer Series in Surface Science Vol. 42 (Springer, Berlin, 2004).

[2] F. Buatier de Mongeot, G. Costantini, C. Boragno, and U. Valbusa, Phys. Rev. Lett. **84**, 2445 (2000).

[3] H.-J. Ernst, F. Fabre, R. Folkerts, and J. Lapujoulade, Phys. Rev. Lett. **72**, 112 (1994).

[4] S.-J. Kahng, B.-Y. Choi, and Y. Kuk, Appl. Surf. Sci. **183**, 76 (2001).

[5] M. Albrecht, H. Fritzsche, and U. Gradmann, Surf. Sci. **294**, 1 (1993).

[6] A. Toma, D. Chiappe, C. Boragno, and F. Buatier de Mongeot, Phys. Rev. B **81**, 165436 (2010).

[7] R. Moroni, D. Sekiba, F. Buatier de Mongeot, G. Gonella, C. Boragno, L. Mattera, and U. Valbusa, Phys. Rev. Lett. **91**, 167207 (2003).

[8] B. Borca *et al.*, Appl. Phys. Lett. **90**, 142507 (2007).

[9] G. Ehrlich and F. Hudda, J. Chem. Phys. **44**, 1039 (1966).

[10] R. L. Schwoebel and E. J. Shipsey, J. Appl. Phys. **37**, 3682 (1966).

[11] J. Villain, J. Phys. I **1**, 19 (1991).

[12] A. Levandovsky and L. Golubović, Phys. Rev. E **76**, 041605 (2007).

[13] M. Tanaka *et al.*, J. Vac. Sci. Technol. B **12**, 1091 (1994).

[14] V. Garcia, H. Jaffres, J. M. George, M. Marangolo, M. Eddrief, and V. H. Etgens, Phys. Rev. Lett. **97**, 246802 (2006).

[15] L. Däweritz, Rep. Prog. Phys. **69**, 2581 (2006).

[16] V. Garcia, Y. Sidis, M. Marangolo, F. Vidal, M. Eddrief, P. Bourges, F. Maccherozzi, F. Ott, G. Panaccione, and V. H. Etgens, Phys. Rev. Lett. **99**, 117205 (2007).

[17] D. H. Mosca, F. Vidal, and V. H. Etgens, Phys. Rev. Lett. **101**, 125503 (2008).

[18] V. M. Kaganer, B. Jenichen, F. Schippan, W. Braun, L. Daweritz, and K. H. Ploog, Phys. Rev. B **66**, 045305 (2002).

[19] R. Breitwieser, F. Vidal, I. L. Graff, M. Marangolo, M. Eddrief, J. C. Boulliard, and V. H. Etgens, Phys. Rev. B **80**, 045403 (2009).

[20] I. Horcas *et al.*, Rev. Sci. Instrum. **78**, 013705 (2007).

[21] M. Kästner *et al.*, J. Vac. Sci. Technol. B **18**, 2052 (2000).

[22] M. Kästner *et al.*, Surf. Sci. **460**, 144 (2000).

[23] M. Sacchi, M. Marangolo, C. Spezzani, L. Coelho, R. Breitwieser, J. Milano, and V. H. Etgens, Phys. Rev. B **77**, 165317 (2008).

[24] M. Sacchi, M. Marangolo, C. Spezzani, R. Breitwieser, H. Popescu, R. Dealaunay, B. Rache Salles, M. Eddrief, and V. H. Etgens, Phys. Rev. B **81**, R220401 (2010).